SCIENCE CHINA
Information Sciences

• **Supplementary File** •

A physical channel-potential and drain-current model for asymmetric dual-gate a-IGZO TFTs

Minxi CAI & Ruohe YAO*

School of Electronic and Information Engineering, South China University of Technology, Guangzhou 510641*, China*

Appendix A Detailed derivation of drain current expression

The introduced effective term in (12) of our letter satisfies

$$E = \mp\sqrt{\alpha_{\mathrm{eff}}^{'} + (F_{\mathrm{t}} + F_{\mathrm{f}})\exp\left(\frac{\varphi - V_{\mathrm{CH}}}{\theta\varphi_{\mathrm{eff}}^{'}}\right)}, \tag{A1}$$

where

$$\alpha_{\mathrm{eff}}^{'} = \frac{C_{\mathrm{oxB}}^{2}}{\varepsilon_{\mathrm{s}}^{2}}(V_{\mathrm{GBf}} - \varphi_{\mathrm{B}})^{2} - (F_{\mathrm{t}} + F_{\mathrm{f}})\exp\left(\frac{\varphi_{\mathrm{B}} - V_{\mathrm{CH}}}{\theta\varphi_{\mathrm{eff}}^{'}}\right), \tag{A2}$$

and

$$\xi\,(F_{\mathrm{t}} + F_{\mathrm{f}})\exp\left(\frac{\varphi - V_{\mathrm{CH}}}{\theta\varphi_{\mathrm{eff}}^{'}}\right) = F_{\mathrm{t}}\exp\left(\frac{\varphi - V_{\mathrm{CH}}}{\varphi_{\mathrm{t}}}\right) + F_{\mathrm{f}}\exp\left(\frac{\varphi - V_{\mathrm{CH}}}{\varphi_{\mathrm{th}}}\right). \tag{A3}$$

Thus ξ and θ can be defined by (A1) and (A3). By evaluating the partial derivative of (A1) as in (11) and substituting the result into (12) in our letter, one can obtain

$$\exp\left(\frac{\varphi - V_{\mathrm{CH}}}{\varphi_{\mathrm{th}}}\right) = \frac{\varphi_{\mathrm{t}}}{\varphi_{\mathrm{t}} - \varphi_{\mathrm{th}}}\frac{\varphi_{\mathrm{th}}}{F_{\mathrm{f}}}\left[\frac{\mathrm{d}\alpha}{\mathrm{d}V_{\mathrm{CH}}} - \frac{\xi\theta\varphi_{\mathrm{eff}}^{'}}{\varphi_{\mathrm{t}}}\frac{\mathrm{d}\alpha_{\mathrm{eff}}^{'}}{\mathrm{d}V_{\mathrm{CH}}} - \left(1 - \frac{\xi\theta\varphi_{\mathrm{eff}}^{'}}{\varphi_{\mathrm{t}}}\right)2E\frac{\partial E}{\partial V_{\mathrm{CH}}}\right]. \tag{A4}$$

The drain current expression in (10) is rewritten with (A4) as

$$I_{\mathrm{DS}} = \frac{\mu W}{L}\frac{qN_{\mathrm{f}}\varphi_{\mathrm{t}}\varphi_{\mathrm{th}}}{F_{\mathrm{f}}\,(\varphi_{\mathrm{t}} - \varphi_{\mathrm{th}})}\left[\int_{0}^{V_{\mathrm{DS}}}\int_{\varphi_{\mathrm{B}}}^{\varphi_{\mathrm{T}}}\frac{1}{-E}\left(\frac{\mathrm{d}\alpha}{\mathrm{d}V_{\mathrm{CH}}} - \frac{\xi\theta\varphi_{\mathrm{eff}}^{'}}{\varphi_{\mathrm{t}}}\frac{\mathrm{d}\alpha_{\mathrm{eff}}^{'}}{\mathrm{d}V_{\mathrm{CH}}}\right)\mathrm{d}\varphi\mathrm{d}V_{\mathrm{CH}} + \int_{0}^{V_{\mathrm{DS}}}\int_{\varphi_{\mathrm{B}}}^{\varphi_{\mathrm{T}}}2\left(1 - \frac{\xi\theta\varphi_{\mathrm{eff}}^{'}}{\varphi_{\mathrm{t}}}\right)\frac{\partial E}{\partial V_{\mathrm{CH}}}\mathrm{d}\varphi\mathrm{d}V_{\mathrm{CH}}\right]. \tag{A5}$$

Since α and $\alpha_{\mathrm{eff}}^{'}$ are independent of φ or x, the first integral in (A5) can be worked out directly as

$$\int_{0}^{V_{\mathrm{DS}}}\int_{\varphi_{\mathrm{B}}}^{\varphi_{\mathrm{T}}}\frac{1}{-E}\left(\frac{\mathrm{d}\alpha}{\mathrm{d}V_{\mathrm{CH}}} - \frac{\xi\theta\varphi_{\mathrm{eff}}^{'}}{\varphi_{\mathrm{t}}}\frac{\mathrm{d}\alpha_{\mathrm{eff}}^{'}}{\mathrm{d}V_{\mathrm{CH}}}\right)\mathrm{d}\varphi\mathrm{d}V_{\mathrm{CH}} = t_{\mathrm{s}}\left(\alpha - \frac{\xi\theta\varphi_{\mathrm{eff}}^{'}}{\varphi_{\mathrm{t}}}\alpha_{\mathrm{eff}}^{'}\right)\Bigg|_{0}^{V_{\mathrm{DS}}}. \tag{A6}$$

And the second integral in (A5) can be simplified into four single integrals by splitting the integral region and then changing the order of the integral

$$\int_{0}^{V_{\mathrm{DS}}}\int_{\varphi_{\mathrm{B}}}^{\varphi_{\mathrm{T}}}2\left(1 - \frac{\xi\theta\varphi_{\mathrm{eff}}^{'}}{\varphi_{\mathrm{t}}}\right)\frac{\partial E}{\partial V_{\mathrm{CH}}}\mathrm{d}\varphi\mathrm{d}V_{\mathrm{CH}} = 2\left(1 - \frac{\xi\theta\varphi_{\mathrm{eff}}^{'}}{\varphi_{\mathrm{t}}}\right)\left(\int_{\varphi_{\mathrm{B0}}}^{\varphi_{\mathrm{BL}}}E_{\mathrm{B}}\mathrm{d}\varphi - \int_{\varphi_{\mathrm{T0}}}^{\varphi_{\mathrm{TL}}}E_{\mathrm{T}}\mathrm{d}\varphi + \int_{\varphi_{\mathrm{BL}}}^{\varphi_{\mathrm{TL}}}E_{\mathrm{L}}\mathrm{d}\varphi - \int_{\varphi_{\mathrm{B0}}}^{\varphi_{\mathrm{T0}}}E_{0}\mathrm{d}\varphi\right), \tag{A7}$$

where $\varphi_{\mathrm{TL(T0)}}$ and $\varphi_{\mathrm{BL(B0)}}$ are the φ_{T} and φ_{B} at $V_{\mathrm{CH}}{=}V_{\mathrm{DS}}(V_{\mathrm{CH}}{=}0)$, $E_{\mathrm{T(B)}}$ is the electric field at the top(bottom) surface, $E_{\mathrm{L(0)}}$ is the electric field at $V_{\mathrm{CH}}{=}V_{\mathrm{DS}}(V_{\mathrm{CH}}{=}0)$, respectively. After some regular mathematical procedures similar to those in [1, 2], the drain current is finally expressed as

$$\begin{aligned} I_{\mathrm{DS}} = \delta\frac{\mu W}{L}\frac{qN_{\mathrm{f}}\varphi_{\mathrm{t}}\varphi_{\mathrm{th}}}{F_{\mathrm{f}}\,(\varphi_{\mathrm{t}} - \varphi_{\mathrm{th}})}\Bigg\{t_{\mathrm{s}}\left[(\alpha_{\mathrm{L}} - \alpha_{0}) - \frac{\xi\theta\varphi_{\mathrm{eff}}^{'}}{\varphi_{\mathrm{t}}}\left(\alpha_{\mathrm{effL}}^{'} - \alpha_{\mathrm{eff0}}^{'}\right)\right] + \left(1 - \frac{\xi\theta\varphi_{\mathrm{eff}}^{'}}{\varphi_{\mathrm{t}}}\right) \\ \cdot\left[\frac{C_{\mathrm{oxB}}}{\varepsilon_{\mathrm{s}}}(\varphi_{\mathrm{BL}} - \varphi_{\mathrm{B0}})(2V_{\mathrm{GBf}} - \varphi_{\mathrm{BL}} - \varphi_{\mathrm{B0}}) + \frac{C_{\mathrm{oxT}}}{\varepsilon_{\mathrm{s}}}(\varphi_{\mathrm{TL}} - \varphi_{\mathrm{T0}})(2V_{\mathrm{GTf}} - \varphi_{\mathrm{TL}} - \varphi_{\mathrm{T0}}) + 2\,(K_{\mathrm{L}} - K_{0})\right]\Bigg\}, \end{aligned} \tag{A8}$$

* Corresponding author (email: phrhyao@scut.edu.cn)

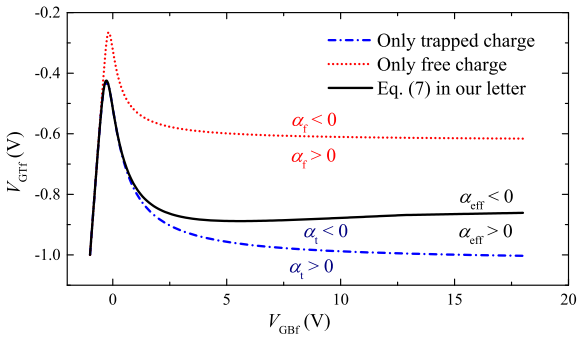

Figure B1 Critical voltage curves of TG with only the trapped or free charges being considered, and the results from (7) ($V_{\rm CH}$=0 V).

Table B1 Geometrical and physical parameters used in the model validation

Parameter	W/L	$C_{\rm oxB}$	$C_{\rm oxT}$	$t_{\rm s}$	$N_{\rm C}$	$N_{\rm TA}$	$\varphi_{\rm F0}$	$T_{\rm t}$	T	μ
(Unit)	(μm/μm)	(nF/cm^2)	(nF/cm^2)	(nm)	(cm^{-3})	(cm^{-3})	(V)	(K)	(K)	(cm^2/Vs)
Value	100/50	34.53	17.27	50	5.2×10^{18}	3.0×10^{18}	0.11	500	300	15

which is the (13) in our letter, where $\alpha_{\rm L(0)}$ and $\alpha'_{\rm effL(eff0)}$ are the α and $\alpha'_{\rm eff}$ at $V_{\rm CH}$=$V_{\rm DS}$($V_{\rm CH}$=0), and

$$K_{\rm L|0}=\begin{cases} 2\theta\varphi'_{\rm eff}\left[\left(2E_{\rm mL|m0}-E_{\rm TL|T0}-E_{\rm BL|B0}\right)+\sqrt{-\alpha'_{\rm effL|eff0}}\left(2\beta_{\rm mL|m0}-\beta_{\rm TL|T0}-\beta_{\rm BL|B0}\right)\right], & \alpha'_{\rm effL|eff0}<0 \\ 2\theta\varphi'_{\rm eff}\left[\left(E_{\rm TL|T0}-E_{\rm BL|B0}\right)-\sqrt{\alpha'_{\rm effL|eff0}}\left(\beta^*_{\rm TL|T0}-\beta^*_{\rm BL|B0}\right)\right], & \alpha'_{\rm effL|eff0}>0 \end{cases}, \quad \text{(A9)}$$

$$E_{\rm TL|BL|mL}=\sqrt{\alpha'_{\rm effL}+(F_{\rm t}+F_{\rm f})\exp\left(\frac{\varphi_{\rm TL|BL|mL}-V_{\rm DS}}{\theta\varphi'_{\rm eff}}\right)}, \quad \text{(A10)}$$

$$E_{\rm T0|B0|m0}=\sqrt{\alpha'_{\rm eff0}+(F_{\rm t}+F_{\rm f})\exp\left(\frac{\varphi_{\rm T0|B0|m0}}{\theta\varphi'_{\rm eff}}\right)}, \quad \text{(A11)}$$

$$\beta^{(*)}_{\rm TL|BL|mL}=\arcsin\left(\rm h\right)\left[\sqrt{\frac{(-)-\alpha'_{\rm effL}}{(F_{\rm t}+F_{\rm f})}}\exp\left(-\frac{\varphi_{\rm TL|BL|mL}-V_{\rm DS}}{2\theta\varphi'_{\rm eff}}\right)\right], \quad \text{(A12)}$$

$$\beta^{(*)}_{\rm T0|B0|m0}=\arcsin\left(\rm h\right)\left[\sqrt{\frac{(-)-\alpha'_{\rm eff0}}{(F_{\rm t}+F_{\rm f})}}\exp\left(-\frac{\varphi_{\rm T0|B0|m0}}{2\theta\varphi'_{\rm eff}}\right)\right], \quad \text{(A13)}$$

in which $\varphi_{\rm mL(m0)}$ is the $\varphi_{\rm m}$ in our letter at $V_{\rm CH}$=$V_{\rm DS}$($V_{\rm CH}$=0). The δ in (A8) or (13) is a differentiable step-like function with the form of $\delta=(1/2)\{\tanh[\gamma(V_{\rm GBf}-V_{\rm sg})]+1\}$, where γ is a weight parameter and $V_{\rm sg}$ is the $V_{\rm GBf}$ when $\xi\theta\varphi'_{\rm eff}/\varphi_{\rm t}$ equals 1.

Appendix B Verification of the potential model

Figure B1 shows the critical voltage curves of TG with only the trapped charges, free charges and effective characteristic temperature-based results by (7) in our letter, where the $\alpha_{\rm t(f)}$ is the respective coupling factor in (1) considering only the trapped(free) charges. Parameters used in the model validation are listed in Table B1. The critical voltage curve calculated by (7) lies between the two curves with only trapped or free charges being considered. When the applied DG bias point ($V_{\rm GBf}$, $V_{\rm GTf}$) locates above the curves, electric fields generated by $V_{\rm GBf}$ and $V_{\rm GTf}$ are weakened and cancelled in the channel layer. Thus, the respective coupling factor is negative, and the potential solution has the trigonometric form as shown in Figure 1(a) in our letter, also known as the F0 case [3]. In contrast, when the applied DG bias is below the curves, the coupled electric field has no change in polarity within the channel region, as shown in Figure 1(b), and the coupling factor is positive. Therefore, the hyperbolic solution or the P0 case should be applied. Bias points right on the curves correspond to critical conditions, where either form of the solutions can be chosen.

Figure B2(a) gives the bottom-surface potential under various $V_{\rm GTf}$ and $V_{\rm GBf}$ by solving (5) in our letter, in which the $\varphi_{\rm Bcr}$ in (6) is used as the initial guess [4,5], and the Levenberg-Marquardt algorithm is adopted, resulting in a convergent and efficient solution. The modeling results fit well with the exact numerical results from (1) and (2). Figure B2(b) shows the errors between the modeled and numerical results in Figure B2(a), with the maximum error no more than 2.7×10^{-3} V. Figures B3(a) and B3(b) give comparisons of the modeled and numerical potential distributions along the x-direction at various $V_{\rm GTf}$ and $V_{\rm GBf}$. As discussed in Figure B1, the potential distributions in Figure B3 have two forms according to the applied DG biases. The potential profile with an extremum indicates the F0 case and the monotonic potential profile is the P0 case. It is observed in Figure B3(a) that $\varphi_{\rm B}$ is notably modified by $V_{\rm GTf}$, because the bottom surface is depleted

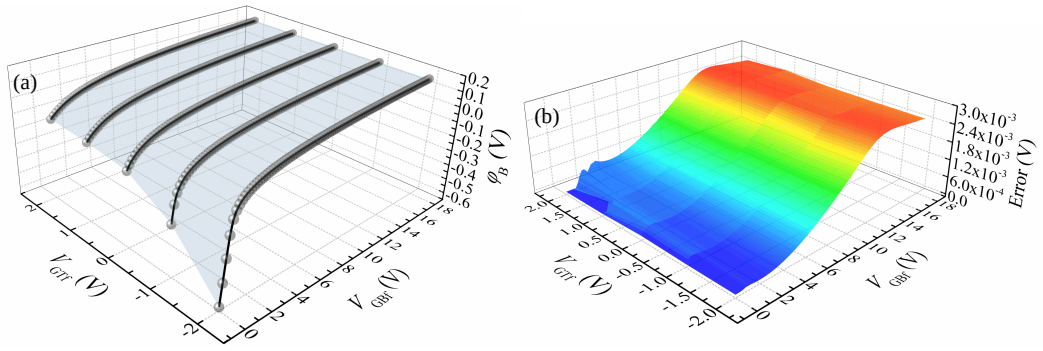

Figure B2 (a) Variations of φ_B with V_{GBf} under V_{GTf}=-2, -1, 0, 1, 2 V and V_{CH}=0 V, in which the surface with lines are results from (5) and scatters are exact numerical results from (1) and (2) in our letter; (b) errors between the modeled and numerical results of φ_B in Figure B2(a). Parameters used are listed in Table B1.

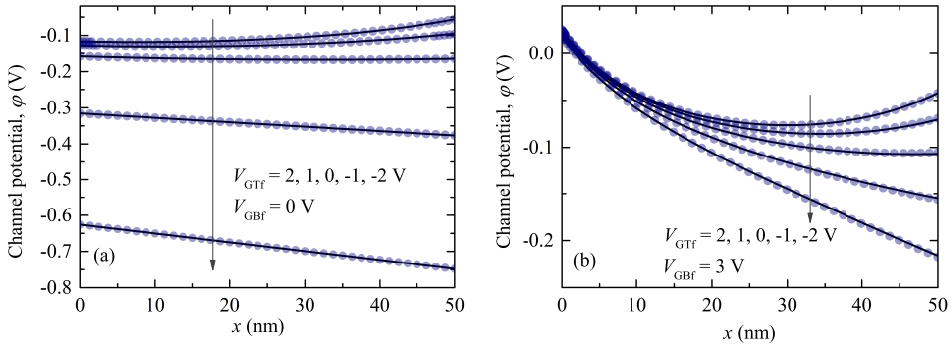

Figure B3 Channel potential distributions under various V_{GTf} with (a) V_{GBf}=0 V and (b) V_{GBf}=3 V (V_{CH}=0 V), where lines are the modeling results by (4) and scatters are exact numerical results from (1) and (2) in our letter. Parameters used are list in Table B1.

or weakly accumulated under V_{GBf}=0 V. The electric field of TG can penetrate through the a-IGZO layer and thus affect φ_B, noticing that the top surface is not in strong accumulation as well. However, as can be seen in Figure B3(b), φ_B is nearly unchanged with V_{GTf} under V_{GBf}=3 V. This is attributed to accumulated carriers at the bottom surface by V_{GBf}, which screens the electric field of TG. In this case, φ_B depends more on V_{GBf} and is less likely to be manipulated by the TG field. It is also shown in Figures B3(a) and B3(b) that the increment of the channel potential slows down as the V_{GTf} increases from -2 V to 2 V, or as the V_{GBf} increases from 0 V to 3 V. This is also related with the transition from depletion to accumulation near the top or bottom surfaces, which results in weakened coupling and diminished effect of each gate on the opposite surface.

Appendix C Verification of the drain current model

Figures C1(a) and C1(b) are transfer curves and output curves of the BG-driven device calculated by (A8) or (13) in our letter, compared with numerical results by (10) under various TG voltages. In Figure C1(a), the transfer curve exhibits parallel shift to positive(negative) direction with decreasing(increasing) V_{GTf}, which is related to the expelling and attraction of carriers by the TG field. A further validation of this drain current model is given in Figure C2 with available experiment data [6]. For DG a-IGZO TFTs, the above parallel shift of transfer curves with almost no change in the subthreshold slope can be explained by the absence of the hole accumulation layer [6]. In the output curves in Figure C1(b), the saturation takes place earlier with the decreasing V_{GTf}, owing to the increased threshold voltage. The insets in Figures C1(b) and C2 show the respective ξ and θ used in calculating the drain current.

Figure C3 shows the transfer curves under various a-IGZO layer thicknesses, in which a crossover region is clearly found. With the decreasing t_s, the drain current increases above the crossover region and drops more quickly (i.e. shows steeper subthreshold slope) below the crossover region, which becomes significant when the t_s is less than 20 nm. The bulk accumulation (BA) a-IGZO TFTs have been widely reported with DG-driving scheme [7, 8], showing remarkable improvement on their DC performances once the BA is achieved by reducing the active layer thickness in adequate. Results in Figure C3 show that the bulk accumulation/depletion also happens in the single gate (SG)-driven DG devices, which can also be seen in the inset of Figure C3. The potential profile near the bottom surface stays almost unchanged when the t_s decreases from 100 nm to 50 nm, whereas begins to increase significantly with t_s lower than 20 nm (especially in the bulk), indicating the extension of accumulation layer throughout the a-IGZO body.

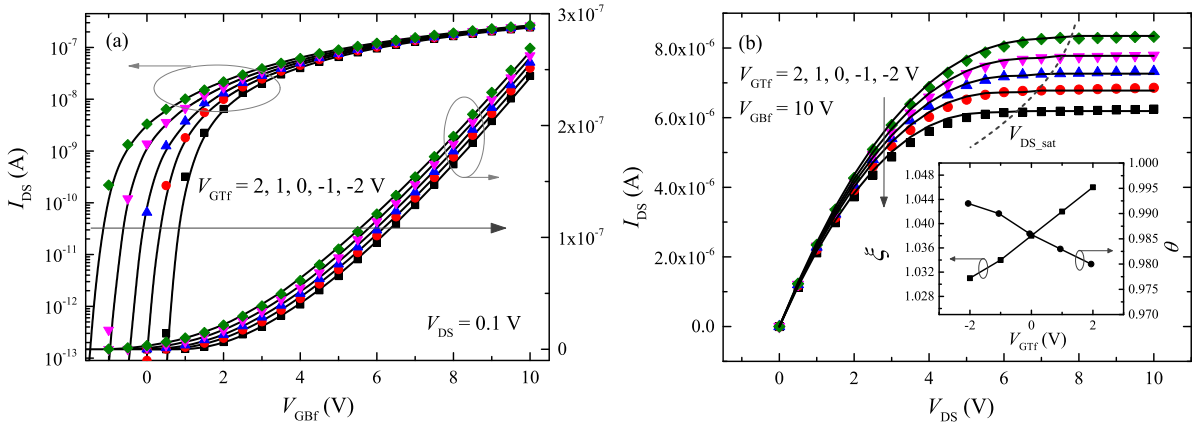

Figure C1 Comparisons between the proposed model (lines by (A8) or (13)) and the numerical results (scatters by (10)) on (a) transfer curves and (b) output curves under various V_{GTf}, where V_{DS_sat} denotes the saturation voltage. The inset shows the ξ and θ used in calculating the drain current. Parameters used are listed in Table B1.

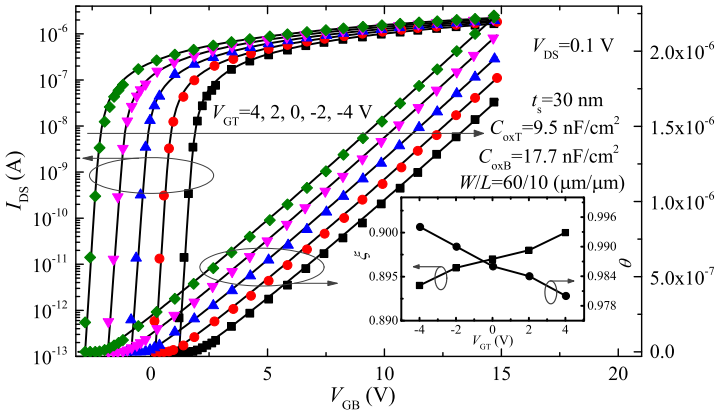

Figure C2 Comparisons between the proposed model (lines by (A8) or (13)) and experiment data [6] on transfer curves under various TG voltages. Parameters used in modeling: N_{TA}=1.5×10^{18} cm^{-3}, T_t=390 K, others are given in Figure C2 and Table B1. The flat-band voltage of the TG(BG) is calculated by $V_{fbT(B)} = \phi_{msT(B)} - \varphi_{F0}$, in which the work-function difference ($\phi_{msT(B)}$) between TG(BG) and semiconductor can be obtained according to [6]. The inset shows the ξ and θ used in calculating the drain current.

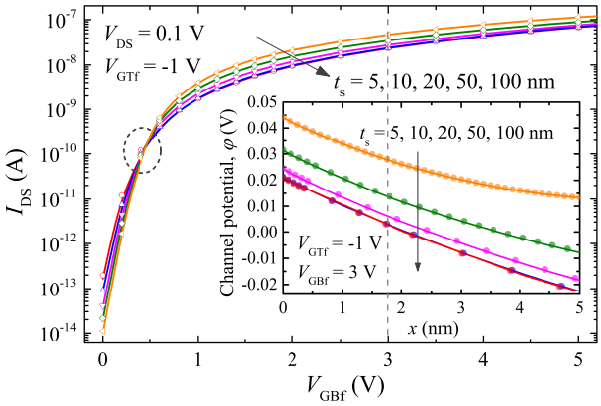

Figure C3 The calculated transfer curves under various t_s, in which lines are calculated by (A8) or (13) and scatters are numerical results by (10). The inset is the modeled (lines) and numerical (scatters) potential profiles near the bottom surface. Parameters used are listed in Table B1.

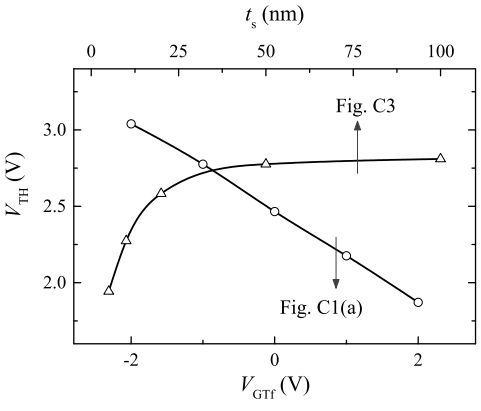

Figure C4 Variations of V_{TH} with V_{GTf} in Figure C1(a) and with t_s in Figure C3.

For the transfer characteristics in Figures C1(a) and C3, by defining the BG voltage at the drain current of 10^{-8} $\frac{W}{L}$ A as the threshold voltage ($V_{\rm TH}$), variations of $V_{\rm TH}$ along with $V_{\rm GTf}$ and $t_{\rm s}$ are shown in Figure C4. The $V_{\rm TH}$ changes almost linearly with $V_{\rm GTf}$, which is consistent with the analysis in Figure C1 and results in the literature [9, 10]. The $V_{\rm TH}$ of devices in Figure C3 increases with increasing $t_{\rm s}$ from 5 nm, and gradually saturates when $t_{\rm s}$ keeps increasing, as shown in Figure C4, which agrees with the results for the enhancement-mode device reported in [11]. The slight increase of $V_{\rm TH}$ with $t_{\rm s}$ at first could be explained by the increased total amount of trap states, since uniformly distributed density of states is assumed in the a-IGZO layer. The calculated carrier concentration (N) in this model under thermal equilibrium is 1.16×10^{16} cm^{-3}, which gives the extrinsic Debye length (λ= $(\frac{\varepsilon_{\rm s}kT}{q^2N})^{1/2}$) of around 35 nm. Thus, the gate-field-induced band bending can extend to the whole active layer when $t_{\rm s}$ is less than 35 nm, where the drain current and threshold voltage depend notably on the active layer thickness. And this explains why no obvious change of $V_{\rm TH}$ is observed when $t_{\rm s}$ exceeds the Debye length for the device in Figure C3. It can be concluded that appropriately reducing the thickness of the active layer improves the DC performances also for the SG-driven DG a-IGZO TFTs.

References

1 Ortiz-Conde A, Herrera R, Schmidt P E, et al. Long-channel silicon-on-insulator MOSFET theory. Solid State Electron, 1992, 35: 1291–1298

2 Ortiz-Conde A, Garca Snchez F J, Muci J. Rigorous analytic solution for the drain current of undoped symmetric dual-gate MOSFETs. Solid State Electron, 2005, 49: 640–647

3 Shi X, Wong M. Analytical solutions to the one-dimensional oxide-silicon-oxide system. IEEE Trans Electron Dev, 2003, 50: 1793–1800

4 Shangguan W Z, Au Yeung T C, Zhu Z M, et al. General analytical Poisson solution for undoped generic two-gated metal-oxide-semiconductor field-effect transistors. Appl Phys Lett, 2007, 90: 012110

5 Sahoo A, Thakur P K, Mahapatra S. A computationally efficient generalized Poisson solution for independent double-gate transistors. IEEE Trans Electron Dev, 2010, 57: 632–636

6 Baek G, Abe K, Kuo A, et al. Electrical properties and stability of dual-gate coplanar homojunction DC sputtered amorphous indium-gallium-zinc-oxide thin-film transistors and its application to AM-OLEDs. IEEE Trans Electron Dev, 2011, 58: 4344–4353

7 Mativenga M, An S, Jang J. Bulk accumulation a-IGZO TFT for high current and turn-on voltage uniformity. IEEE Electron Dev Lett, 2013, 34: 1533–1535

8 Chen T L, Huang K C, Lin H Y, et al. Enhanced current drive of double-gate -IGZO thin-film transistors. IEEE Electron Dev Lett, 2013, 34: 417–419

9 Abe K, Takahashi K, Sato A, et al. Amorphous In-Ga-Zn-O dual-gate TFTs: Current-voltage characteristics and electrical stress instabilities. IEEE Trans Electron Dev, 2012, 59: 1928–1935

10 Gu P, Chen J, Xie D, et al. Mutual interaction of voltage between top gate and bottom gate for a-IGZO TFT. SID Symp Dig Tech Pap, 2017, 48: 1287–1290

11 Jeong J, Hong Y. Debye length and active layer thickness-dependent performance variations of amorphous oxide-based TFTs. IEEE Trans Electron Dev, 2012, 59: 710–714